Structural, Spectroscopic Characterization and Docking Study of 4-Amino-3-Nitropyridine with Experimental Technique and Quantum Chemical Calculations

Rasheed .M.P[1*] S.Seshadri [2] R sangeetha [3] Satheeshkumar MK[4]

[1,3] *(Research Scholar, PG and Research Department of Physics, Urumudhanalakshmi College ,Trichy-19, India)*
[2]*(Associate Professor and HOD,PG and Research Department of Physics,Urumudhanalakshmi College ,Trichy-19)*
[4]*(Associate Professor, PG and Research Department of Physics, Govt Brennan College, Thalassery, Kerala, India)*

Abstract: **The FTIR and FT Raman spectra of 4-amino-3-nitropyridine (4a3np) have been recorded in the region 4000-400 cm^{-1} and 4000-50 cm^{-1}. The optimized geometry, intensity and frequency of the vibrational bands of the compound was obtained by density functional theory using B3LYP/6-311++G(d,p) basis set. The harmonic vibrational frequencies were calculated and scaled values have been compared with experimental FTIR and FT Raman spectra. The observed and calculated frequencies are found to be in good agreement. A detailed interpretation of the infrared and raman spectra were also reported based on potential energy distribution (PED). Electronic properties , HOMO and LUMO energies were calculated and UV visible spectrum of the compound was recorded by time dependent density functional theory approach (TD-DFT). The calculated HOMO and LUMO energies show that charge transfer occurs within the molecule. The ^{1}H and ^{1}C nuclear magnetic resonance (NMR) chemical shifts of 4A3NP were calculated using GIAO approach by applying B3LYP method. The dipole moment, polarizability and first order hyperpolarizability , Mullikan charges and natural atomic charges of title molecule were calculated using DFT calculations. The chemical reactivity and thermodynamic properties of 4A3NP at different temperatures were calculated. Docking studies of the title compound were performed to predict the proffered binding orientation, affinity and activity of the given compound. The title compound was docked in to active site of proteins 4YPO and 5NCJ which belongs to the class of proteins exhibiting the property of anti tuberculosis. In both cases estimated inhibition constant, minimum estimated free binding energy and final intermolecular energy were seen in the interaction.**

Keywords: FTIR;FT-Raman;UV-Vis; NMR;HOMO LUMO; 4A3NP

High lights

- **DFT calculation provides significant result with high accuracy.**
- **Vibrational assignments were performed using FT IR and FT Raman spectra.**
- **Comparison of experimental and theoretical data confirms the efficiency of calculations .**
- **The electronic and HOMO - LUMO energies were carried out .**
- **^{1}H and ^{13}C NMR chemical shift were calculated using GIAO method.**
- **Molecular docking studies were reported.**

[*]***Corresponding Author: Rasheed M P, e-mail: reshi3355@gmail.com , Tel: +91 9947234807***

I. INTRODUCTION

Pyridine, also called azabenzene and azine, is a heterocyclic aromatic tertiary amine characterized by a six membered ring structure composed of five carbon atoms and one Carbon - Hydrogen unit in the benzene ring being replaced by a nitrogen atom. The simplest member of the pyridine family is pyridine itself. It is colourless, flammable, toxic liquid with an unpleasant odour, miscible with water and with most organic solvents, boils at 115 C. It is made from crude coal tar or from other chemicals based on acetaldehyde and ammonia. Amino pyridines are obtained from pyridine, when an amino group is replaced a hydrogen attached to the ring

The pyridine ring system occurs in the structures of many natural products, pharmaceutical and agrochemical compounds, and other commercial substances. Pyridine has been used very frequently as a proton acceptor in studies involving hydrogen bonded complexes [1,2]. Pyridine derivatives are used as non-linear materials [3] and photo chemicals [4-9]. Analysis of the scientific and patent literature indicates that the amino group is used to create a wide range of the drugs and products for agriculture [10,11]. Some pyridine derivatives are patented and widely used in medicine as the anti androgenic and hypertensive drugs [12]. Many substituted pyridines are involved in bioactivities with applications in pharmaceutical drugs and agricultural products [13-15]. Pyridine derivatives act as anaesthetic agents, drugs for certain brain diseases, and prodrugs for treating neuronal damage caused by stroke. They also underpin analgesics for acute and chronic pain, treatment for tinnitus, depression, and even diabetic neuropathy. The picoline derivatives prepared from amino pyridine derivatives have been shown to have cholesterol lowering properties, anti-cancer and anti-inflammatory agents. Antimicrobial preparations based on pyridine derivatives are of great interest and are used in medicine and in agriculture [16]. 4-Amino-3-nitropyridine is a pyridine derivative and it is used to treat some symptoms met in Lambert–Eaton myasthenia syndrome. It was shown efficient to reduce a form of variable muscle weakness and fatigability typical of the disease and correlated to a block of acetylcholine release. It has anti

tuberculosis properties. Our molecule 4A3NP having the molecular formula $C_5H_5N_3O_2$ has the Boiling point: 203-207 °C **.** It is a yellow crystalline powder.

II. EXPERIMENTAL DETAILS

The fine sample of 4A3NP was purchased from Sigma Aldrich Chemicals, UK, and used as such for the spectral measurements like FT IR and FT Raman spectra. The room temperature FTIR spectrum of the title compound was measured in the 4000- 400 cm^{-1} region at a resolution of ±1 cm^{-1}, using a BRUKER IFS-66V vacuum Fourier transform spectrometer equipped with a Mercury Cadmium Telluride (MCT) detector, a KBr beam splitter and global source.

The FT-Raman spectra was also recorded in the range between 4000-50 cm^{-1} by the instrument with FRA 106 Raman module equipped with Nd:YAG laser source with 200 mW power operating at 1.064 nm. The reported wave numbers are expected to be accurate within ±1 cm^{-1}.

III. COMPUTATIONAL DETAILS

For meeting the requirements of accuracy and computing economy, theoretical methods and basis sets were considered. The Density Functional Theory (DFT) has been proved to be extremely useful in treating electronic structure of molecules. The gradient corrected Density Functional Theory (DFT) [17] with the three-parameter hybrid functional Becke3 (B3) [18] for the exchange part and the Lee Yang Parr (LYP) correlation function [19] level of calculations have been carried out in the present investigation, using 6-311++G(d,p) basis sets with GAUSSIAN 09 program [20]package, invoking gradient geometry optimisation [21] on a Intel Core i5-3337U/1.8 GHz processor.

Geometry optimization is the procedure that attempts to find the configuration of minimum energy of the molecule. The procedure calculates the wave function and the energy at a starting geometry and then proceeds to search a new geometry of a lower energy. In the final, minimum energy geometry the force on each atom is zero. The optimized geometry corresponding to the minimum on the potential energy surface have been obtained by solving self consistent field equation iteratively. Harmonic vibrational wave numbers have been calculated using analytic second derivatives to confirm the convergence to minima on the potential energy surface and to evaluate the zero-point vibrational energy [22]. Multiple scaling of the force field has been performed by the SQM procedure [23,24] to offset the systematic errors caused by basis set incompleteness, neglect of electron correlation and vibrational anharmonicity [25].These force fields obtained in Cartesian coordinates and dipole derivatives with respect to atomic displacements were extracted from the archive section of the Gaussian 09 output and transformed to a suitably defined set of internal coordinates (the 'natural coordinates'). Normal coordinate analysis on 4A3NP has been performed to obtain full description of the molecular motion pertaining to the normal modes. The potential energy distributions corresponding to each of the observed frequencies were calculated with the help of MOLVIB-7.0 program [26,27]

The intensities of Raman scattering depend on the square of the infinitesimal change of the polarizability with respect to the normal coordinates. Normal coordinate specifies the instantaneous displacement of an independent mode of oscillation of the system. Each normal coordinate oscillates at a characteristic frequency and is completely unaffected by the other coordinates. The Raman activities (Si) calculated by Gaussian 09 program have been suitably adjusted by the scaling procedure with MOLVIB and subsequently converted to relative Raman intensities (Ii) using the following relationship derived from the basic theory of Raman scattering [28,29].

$$I_i = \frac{f(v_0 - v_i)^4 S_i}{v_i[1 - exp\left(\frac{-hcv_i}{kT}\right)]} \qquad (1)$$

where v_0 is the exciting frequency (in cm^{-1} units); v_i is the vibrational wave number of the i^{th} normal mode; *h*, *c* and *k* are fundamental constants and *f* is a suitably chosen common normalization factor for all peaks intensities.

IV. RESULTS AND DISCUSSION

4.1 Molecular Geometry

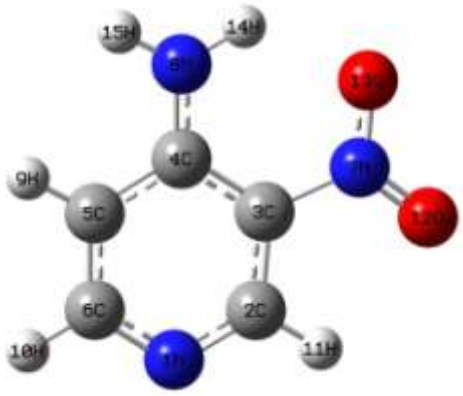

Fig 1. Optimized Structure of 4A3NP along with numbering of atoms

The optimized molecular structure and the labelling of atoms of title compound is obtained from Gaussian 09W and Gauss View 5.0 programs as shown in Figure. 1. The global minimum energies obtained by the DFT structure optimization for 4A3NP for B3LYP/6-31G (d,p) , B3LYP/6-311+G(d,p), and B3LYP/6-311G++(d,p) basis sets respectively are presented in Table 1. This energy difference may be due to the molecules are under different environments.

Table 1-Total energies (in Hartrees) based on B3LYP/6-31 g(d,p) , B3LYP/6-311 + G(d,p) and B3LYP/6-311 + +G(d,p) basis sets for 4A3NP

Basis set	4-Amino-3-nitropyridine
B3LYP/6-31 G(d,p)	-508.11320982
B3LYP/6-311+ G(d,p)	-508.25065661
B3LYP/6-311++ G(d,p)	-508.29797923

Bond length is the distance between the nuclei of two bonded atoms whereas bond angle is the angle formed between two adjacent atoms in a molecule. They always range from 100-180 degrees. Bond angle and bond length are the two important parameters which determine the shape and size of a molecule. The geometry of a molecule can be characterized by analyzing the bond length and bond angle. These parameters can vary in their length depending upon their bond multiplicity. They are shorter for a triple bond than for a single bond. Bond angles too vary in their angles from molecule to molecule depending upon on the electron structures of the molecule.

A dihedral angle or torsion angle is the angle between two planes. It defines the conformations around rotatable bonds. The dihedral angle changes only with the distance between the first and fourth atoms; the other inter atomic distances are controlled by the chemical bond lengths and bond angles. Its value ranges from -180 to +180 degrees. The torsion angle is considered to be positive if a clockwise rotation is performed with the molecule and it will be negative when an anti clockwise rotation is performed with the molecule in its plane[29].The optimized geometrical parameters like bond length, bond angles and dihedral angles are presented in Table 2.

Table 2-Optimized geometrical parameters of 4A3NP obtained by B3LYP/6-31 g(d,p) density functional calculations

Bond	Angstrum (Å)	Bond angle	Degree	Torsional angle	Degree
N8-H14	1.008631	C3-C2-N1	123.53	H14-N8-C4-C5	-180
N8-H15	1.004835	H14-N8-C4	119.37	H15-N8-C4-C5	0
C2-H11	1.078453	H15-N8-H14	120.33	H11-C2-N1-C6	-180
C5-H9	1.081801	H11-C2-N1	117.52	H9-C5-C6-N1	-180
C6-H10	1.080439	H9-C5-C6	120.36	H10-C6-N1-C2	-180
C6-C5	1.376504	H10-C6-N1	115.52	C2-N1-C6-C5	0
N1-C2	1.335028	C2-N1-C6	116.89	C3-C2-N1-C6	0
C3-C2	1.407813	N8-C4-C5	120.33	O12-N7-C3-C4	-180
N8-C4	1.356091	O12-N7-C3	119.27	C4-C5-C6-N1	0
O12-N7	1.268491	N1-C6-C5	123.77	O13-C3-O12-N7	0
N1-C6	1.367878	C4-C5-C6	120.52	N8-C5-C3-C4	0
C4-C5	1.422058	O13-N7-O12	121.81	N7-C4-C2-C3	0
O13-N7	1.286075	N7-C3-C2	117.75		
N7-C3	1.438006				

For numbering of atoms refer Fig. 1

4.2 Assignment of Spectra

FTIR stands for Fourier transform infrared spectroscopy. When IR radiation is passed through a sample, some radiation is absorbed by the sample and some radiation is transmitted. The resulting signal at the detector is a spectrum representing a molecular 'fingerprint' of the sample. The usefulness of infrared spectroscopy arises because different chemical structures produce different spectral fingerprints. Theoretical and experimental FT-IR spectrum of 4A3NP is given in Figure 2

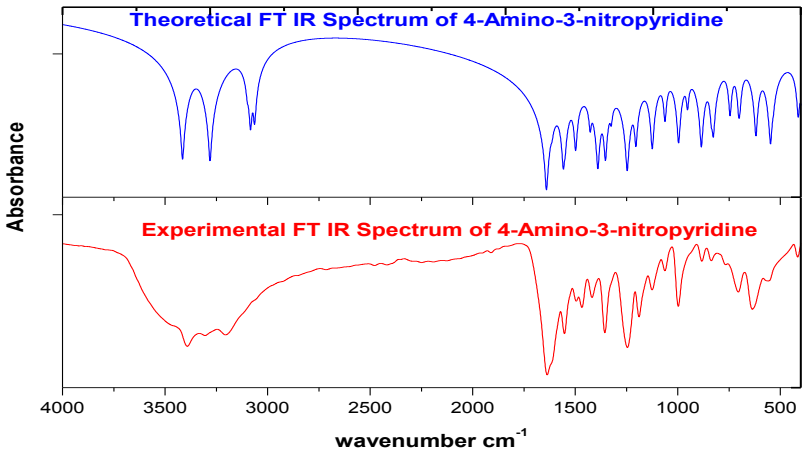

Fig 2. Comparison of Theoretical and experimental FT-IR spectrum of 4A3NP

Raman spectroscopy is a technique which has evolved from what used to be regarded as an interesting research phenomenon into a valuable analytical tool. As a complementary technique to FT-IR, Raman offers benefits that include minimal

sample preparation, the ability to sample through containers, nondestructive analysis, easy analysis of inorganic molecules, and minimal interference from water. Theoretical and experimental FT Raman spectrum of 4A3NP is given in Figure 3. Comparison between the calculated and observed vibrational spectra helps us to understand the observed spectral features.

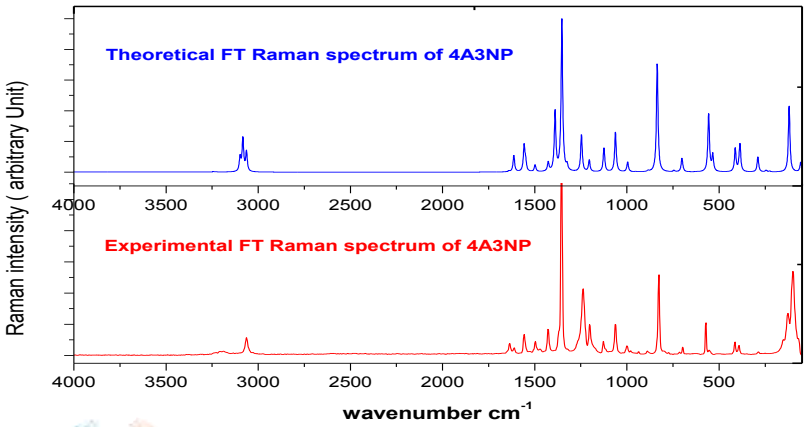

Fig 3. Comparison of Experimental and Theoretical FT-Raman spectrum of 4A3NP

The vibrations of a molecule are given by its normal modes. Each absorption in a vibrational spectrum corresponds to a normal mode. The normal coordinate calculations have been performed to obtain vibrational frequencies and the potential energy distribution for the various modes. In the normal coordinate analysis, the potential energy distribution plays an important role for the characterization of the relative contributions from each internal coordinates to the total potential energy associated with a particular normal coordinate of the molecule. Detailed description of vibrational modes can be given by means of normal coordinate analysis and it also gives a complete picture about the molecular dynamics of amino pyridines. Non-linear molecules have three rotational axes; In general a molecule with N number of atom has 3N-6 normal modes. Our title molecule belongs to C_1 point group symmetry and consists of 15 atoms, which undergo 39 normal modes of vibrations .The total number of 39 fundamental vibrations (3N-6, where N is the number of atoms) are distributed as Γ_{vib} 39 = 27 A' (In plane vibrations; 2N-3) + 12 A" (out of plane vibrations; N-3). The A' modes be polarized while the A" modes be depolarized in the Raman spectra of the compound. The results of our vibrational analysis, viz., calculated unscaled vibrational frequencies and IR intensities, Scaled Quantum Mechanical(SQM) frequencies, potential energy distributions (PED) and assignment of the fundamentals, for the title compound were collected in Table 3.When using computational methods to predict theoretical normal vibrations for relatively complex poly atomic structures, scaling strategies are used to bring computed wave numbers into closer agreement with observed frequencies using the latest version of MOLVIB program.

TABLE 3 - **Assignment of fundamental vibrations of 4A3NP by normal mode analysis based on SQM force field calculations using selective scaled B3LYP/6-31g(d,p)**

No	symmetry species	Observed frequency		Calculated using B3LYP/6-31 G(d,p) force field Freq					Characterisation of normal modes with PED%
		IR (cm^{-1})	Raman (cm^{-1})	Unscaled (cm^{-1})	Scaled (cm^{-1})	IR intensity (K mol^{-1})	Raman activity Si	Raman intensity (Ii)	
1	A'	3391.6	-	3712.2	3392	1.3992	48.38	51.95	νNH(100)
2	A'	3305.1	-	3565.9	3257	342.87	162.45	200.88	νNH (99)
3	A'	3204.9	-	3194.8	3195	61.49	68.7	122.95	νCH (99)
4	A'	-	-	3178.8	3179	1.6293	158.35	288.04	νCH (99)
5	A'	-	3063.6	3158.9	3159	21.469	93.06	172.77	νCH (99)
6	A'	1636.7	-	1656.4	1640	9.6124	6.01	70.09	bHNH(41), νCC(21), CNar(11),
7	A'	-	1635.9	1618.4	1631	5.1583	8.77	108.51	bHNH (41), νCC(17), νNO(17),
8	A'	-	-	1586	1594	84.107	20.58	268.11	CNar(35), νCC(16),bHNH(11),
9	A'	1552.6	1557.4	1556.4	1553	2.5538	17.28	236.11	νNO (36), CNar(19), bCH(17),
10	A'	1495.1	1496.9	1508.9	1506	4.2303	4.54	67.09	bCH (42), νCC(19), νNO(18)
11	A'	1417.9	1427.3	1439.1	1429	7.8992	6.41	106.45	bCH (52), νCC (24),
12	A'	-	-	1385.4	1366	5.5488	4.54	82.81	νCC(36), bCH(21),CNar(16),

13	A'	1355.6	1354.5	1367.8	1350	16.987	127.35	2397.1	νNO (41), νCC (22), νCN (15),
14	A'	-	-	1323.8	1295	20.449	1.83	37.35	bCH (32), νCC (31), bCN (19),
15	A'	-	-	1283.6	1279	29.372	67.5	1482.9	νCC(21),
16	A'	-	1237.5	1226.1	1233	0.0002	16.61	407.46	bCH(27), CNar (23), νCC(19),
17	A'	1124.9	1127.7	1134.7	1118	0.7859	9.54	281.54	bCH(36), νCC(27), νCN(13),
18	A'	1062.6	1062.4	1093.3	1067	13.62	28.84	928.63	bRing(24), νCN(24),CNar(21),
19	A'	-	-	1025.8	1030	12.857	1.94	72.48	gCH(91), tRing(8)
20	A"	-	-	1002.7	981	0.7407	0.3	11.76	gCH (83), tRing (14)
21	A"	997.4	999.37	955.57	897	7.8822	0.15	6.56	bRing (44), bONO(14),
22	A'	882.4	-	895.01	858	5.0935	0.39	19.87	bCNH (50), νCC (21)
23	A'	836.5	-	841.76	848	2.9815	39.49	2322.3	gCH (86),
24	A"	-	826.88	829.3	835	0.8429	0.09	5.49	νCC (32), bRing (27), νCN (15)
25	A"	-	-	719.01	721	3.6474	0.36	30.23	tRing (65), gCN (22)
26	A'	704.7	-	715.78	708	3.7364	2.68	226.38	bRing (64), νCC (15)
27	A"	-	697.35	699.01	695	139.23	0.47	41.69	tNO2 (38), gCN (32), tRing (
28	A"	635.9	-	619.94	638	153.09	0.05	5.86	tNH2 (86)
29	A'	-	572.07	563.57	565	1.1739	12.44	1778.5	bCN(31),bCNO(25),CC(21),bRing(
30	A'	559.4	-	549.7	554	4.9418	0.16	24.74	gCN (57), tRing (34)
31	A"	-	-	542.03	546	14.038	2.98	463.78	bRing (50), νCN (16), νCC
32	A'	415.3	414.08	408.71	415	15.561	5.6	1593.3	bCN (58), bCNO (16)
33	A"	-	392.29	392.35	400	3.6988	0.41	126.7	tRing (52), tNO2 (21), gCN (
34	A'	-	-	381.88	375	4.2118	1.42	468.15	bRing (37), νCN (36), bCN (17)
35	A'	-	-	290.59	305	8.2601	0.8	469.33	bCN (83)
36	A"	-	-	244.64	249	0.0318	0.11	88.22	tNH2 (72), gCN (19)
37	A"	-	-	226.22	233	0.1046	0.04	38.37	tRing(33),tNH2(24),gCN(23),tNO2
38	A"	-	126.83	120.4	122	6.0736	1.16	4155.6	tNH2 (68), gCN (20), tRing (
39	A"	-		55.07	54	2.5386	0.04	766.04	tNO2 (88), tNH2 (9)

(υ) stretching; (b) bending; (g) scissoring and wagging ; (t) torsion ,PED values greater than 10% are given

The RMS error between unscaled (B3LYP/6-311++ g(d,p)) and experimental frequencies are found to be 38.3 cm^{-1}.Root mean square value is obtained in the study using the following expression

$$RMS = \sqrt{\sum_i^n \frac{1}{n-1}(v_i^{calcu} - v_i^{exp})^2} \qquad (2)$$

This is quite obvious since the frequencies calculated on the basis of quantum mechanical force fields usually differ appreciably from observed frequencies. This is partly due to the approximate nature of the quantum mechanical methods and partly due to the neglect of anharmonicity. In order to reproduce the observed frequencies, refinement of scaling factors are applied and optimized via least square refinement algorithm which resulted in a weighted RMS deviation of 7.85 cm^{-1} between the experimental and scaled frequencies.

For 4A3NP, a multiple scale factors are applied in the normal coordinate analysis and the subsequent least square fit refinement, results into the very close agreement between the observed fundamentals and the scaled frequencies (Table 3). Refinement of the scaling factor applied in this study achieved a weighted mean deviation of 4.86 cm^{-1} between the experimental and SQM frequencies. It is beneficial to discuss the vibrational spectra of 4A3NP in terms of characteristic spectral regions were described below in detail.

4.2.1 C-H vibration

The hetero aromatic structure shows the presence of C-H stretching vibrations in the region 3100-3000 cm^{-1} which is the characteristic region [30]. The IR spectrum usually has several bands here while the Raman usually has only one. The 4A3NP has two adjacent and one isolated C-H moieties. In the present study the three expected C-H stretching vibrations correspond to mode Nos. 3, 4 and 5. And hence the weak band appears at 3204.9 cm^{-1} in IR spectrum is assigned to C-H stretching vibrations. The corresponding theoretical value is at 3194.82 cm^{-1} . The weak band at 3063.65 in Raman Spectrum has been assigned to C-H stretching vibration.

The bands due to C-H in-plane ring bending vibrations, interacting somewhat with C-C stretching vibrations, are observed as a number of medium and weak intensity sharp bands in the region 1300-1000 cm^{-1}.Hence bands observed at 1495.1, 1417.9 and 1124.9 cm^{-1} in IR spectrum and the bands observed at 1496.92,1427.39,1237.51 and 1127.74 cm^{-1} in Raman spectrum have been assigned to C-H in plane bending vibrations as shown in Table 3. The C-H out-of-plane bending vibrations are strongly

coupled vibrations and occur in the region 900-667 cm^{-1}.Hence the band appeared at 836.5 cm^{-1} in Raman spectrum has been assigned to C-H out of plane bending vibrations.

4.2.2 C-C vibration

The ring carbon-carbon stretching vibrations investigation occurs in the region in 1625-1430 cm^{-1} [31]. In the present case the bands of C-C stretching vibrations in ring appear at 1636.7 cm^{-1},1552.6 cm^{-1},1495.1 cm^{-1},1417.9 cm^{-1} and 1355.6 cm^{-1},1557.4 cm^{-1},1496.9 cm^{-1} ,1427.3 cm^{-1} and 1354.5 cm^{-1} in FTIR and 1635.9 cm^{-1} in Raman spectra are also consistent with the calculated one. These assignments are in good agreement with the literature [32].

4.2.3 Ring Vibrations

Usually an in-plane deformation vibration is at higher frequencies than the out of plane vibration [33]. In the present study, the bands observed at 997.4 cm^{-1} and 704.7 cm^{-1} in FTIR and 999.37 cm^{-1}, 826.88 cm^{-1} and 572.07 cm^{-1} in FT Raman spectrum respectively are attributed to ring in-plane bending modes. The ring out-of-plane bending mode frequencies are established at 697.35 cm^{-1}, 559.4 cm^{-1} and 392.92 cm^{-1} in FT Raman and FTIR spectra as shown in Table 3

4.2.4 Nitro Group Vibration

Aromatic nitro compounds have strong absorptions due to asymmetric and symmetric stretching vibrations of the nitro group at 1570-1485 cm^{-1} and 1370-1320 cm^{-1} [34-36]. The strong band observed in Raman at 1338 cm^{-1} is assigned to NO_2 asymmetric stretching mode. The symmetric NO_2 stretching is observed in IR as a medium band at 1290 cm^{-1}. The nitro group is capable of bending in a number of different directions and these vibrations give rise to several variable intensity bands at lower wavenumbers. The medium bands in IR at 697 cm^{-1} is assigned to the NO_2 scissoring mode, 737 cm^{-1} at out of plane deformation and that at 544 cm^{-1}, the NO2 rocking vibration.

4.2.5 C-N vibrations

The C-N stretching frequency is a rather difficult task since the mixing of several bands is possible in this region[37]. In our present work, the band observed at 1636.7 cm^{-1} in FTIR spectrum and 1557.48 cm^{-1} in Raman spectrum have been attributed to C-N vibrations. The theoretically computed value of the corresponding C-N stretching vibrations is predicted at 1656.4 cm^{-1} and 1556.4 cm^{-1} respectively and which are scaled to 1640 cm^{-1} and 1553 cm^{-1} . These vibrations are mixed with C-C and N-O stretching and N-H bending vibration as evident from the last column (PED) of Table 3. In this work, the peaks identified at 1355.6 cm^{-1} in FT IR and 1354.5 cm^{-1} in Raman spectrum have been assigned to C-N stretching absorption bands.

4.2.6 Amino group vibrations

Hetrocyclic compounds containing an N-H group exhibit N-H stretching absorption in the region from 3500 cm^{-1} to 3200 cm^{-1} [38] and a weak band at 3100–3070 cm^{-1} for an overtone of the N–H band [39].The position of absorption depends upon the degree of hydrogen bonding and hence upon the physical state of the sample [40]. The nitrogen and hydrogen bonds present in the title molecule will give rise to N-H stretching, in-plane and out-of-plane bending vibrations. For the title compound, the very strong band observed at 3391.6 and 3305.1 cm^{-1} in the IR spectrum have been assigned as N-H stretching mode. The calculated wavenumber for this mode is at 3712.24 cm^{-1} and 3565.96 cm^{-1} respectively in B3LYP method and they are scaled to 3392 cm^{-1} and 3257 cm^{-1} .This mode is a pure stretching mode, and as it is evident from the PED column they are almost contributing 100%. The wavenumber 3712.2 cm^{-1} computed by B3LYP/6-311++G(d,p) method shows the deviation 320.64 cm^{-1} when compared with experimental IR data 3391.6 cm^{-1}. This may be due to intermolecular hydrogen bonds in solid state between the NH group and the N atom present in the ring. This is the reason for the downshift of NH band at 3712 cm^{-1}.The N–H in-plane bending mode observed at 1635.99 cm^{-1} in FT-IR spectrum and 1636.7 cm^{-1} in FT-Raman spectrum . The calculated wave number for these modes are at 1656.42 cm^{-1} and 1618.41 cm^{-1} respectively at B3LYP method and they are scaled to 1640 cm^{-1} and 1631 cm^{-1} respectively. Theoretically predicted values are coinciding very well with the observed frequencies. The PED corresponding to this vibration suggests that these (mode.No.6 and 7) modes are medium modes and exactly contributing to 41% in each case (Table 3).

The weak N-H out of plane bending mode (tNH_2) observed at 635.9 cm^{-1} in FT-IR spectrum and 126.83 cm^{-1} in FT-Raman spectrum. The calculated wavenumber for these modes are at 619.94 cm^{-1} and 120.4 cm^{-1} in B3LYP method and those bands were scaled to 638 cm^{-1} and 122 cm^{-1} respectively. Theoretically predicted values are coinciding very well with the observed frequencies. The PED corresponding to these wagging vibrations suggest that they (mode.Nos.28 and 38) are medium mode and exactly contributing to 86% and 68% respectively (Table 3).

4.3 Electronic properties

The energies of two important molecular orbitals of title molecule, the Highest Occupied Molecular Orbitals (HOMO) and the Lowest Unoccupied Molecular Orbitals (LUMO) were calculated and are presented in Fig. 4. The MO theory treats molecular bonds as a sharing of electrons between nuclei. This theory treats the electrons as localized balloons of electron density. The MO theory says that the electrons are delocalized. That means that they are spread out over the entire molecule.

Both the Highest Occupied Molecular Orbital (HOMO) and the Lowest Unoccupied Molecular Orbital (LUMO) are the main orbital taking part in chemical reaction. The HOMO energy characterizes the ability of electron giving, the LUMO characterizes the ability of electron accepting, and the gap between HOMO and LUMO characterizes the molecular chemical stability [41]. The energy gap between HOMO and LUMO is a critical parameter in determining molecular electrical transport properties because it is a measure of electron conductivity [42]. Molecular orbitals (HOMO and LUMO) and their properties such as energy are very useful for physicists and chemists and are very important parameters for quantum chemistry. This is also used by the frontier electron density for predicting the most reactive position in π electron systems and also explains several types of reaction in conjugated system [43]. This electronic absorption corresponds to the transition from the ground state to the first excited state and is mainly described by one electron excitation from the highest occupied molecular orbital to the lowest unoccupied molecular orbital [44].

While the energy of the HOMO is directly related to the ionization potential, LUMO energy is directly related to the electron affinity.Recently, the energy gap between HOMO and LUMO has been used to prove the bioactivity from intramolecular charge transfer [45,46]. Moreover, lower in the HOMO and LUMO energy gap explains the eventual charge transfer interactions taking place within the molecule. According to B3LYP/6-311++g(d,p) calculation, the energy band gap (translation from HOMO to LUMO) of the molecule is about 3.8939 eV

HOMO energy = - 7.3498 eV
LUMO energy = - 3.4559 eV
HOMO – LUMO energy gap = 3.8939 eV

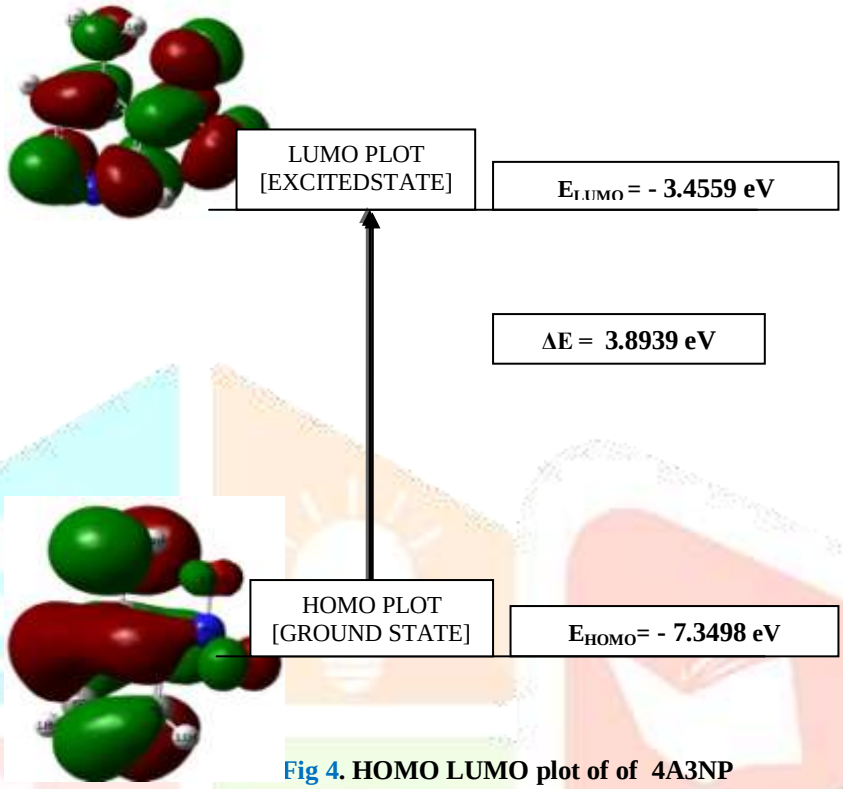

Fig 4. HOMO LUMO plot of of 4A3NP

4.4 UV-Vis spectral analysis

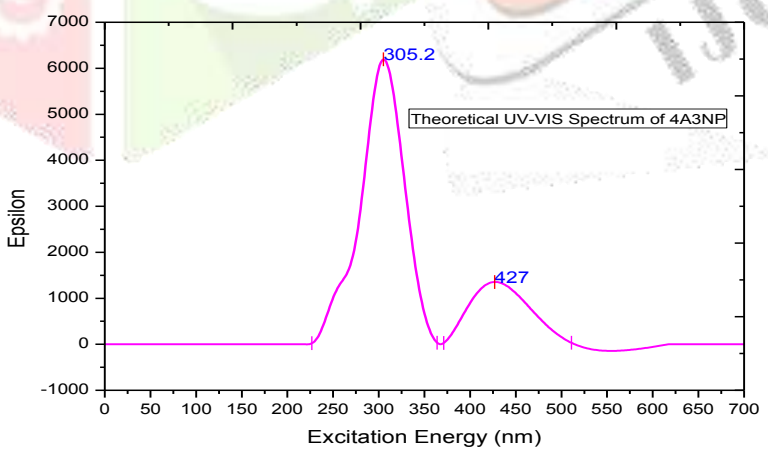

Fig.5. The UV-Visible spectrum of 4A3NP

Ultraviolet spectral analysis of 4A3NP have been investigated by the Time Dependant Density Functional Density Theory (TD-DFT) B3LYP/6-311++G(d,p) method. TD-DFT is able to detect accurate absorption wavelengths at a relatively small computing time which correspond to vertical electronic transitions computed on the ground state geometry, especially in the study of solvent effect [47-49]; Thus TD-DFT method is used with B3LYP function and 6-311++G(d,p) basis set for vertical excitation energy of electronic spectra. The excitation energies, wave length and oscillator strengths for the title molecule at the optimized geometry in the ground state were obtained in the frame work of TD-DFT calculations with the B3LYP/6-311++G(d,p) method. The theoretical electronic excitation energies, wavelength of the excitation and oscillator strengths were calculated and listed in TABLE 4 and the Theoretical UV-Visible spectrum is shown in Figure 5. TD-DFT methods are computationally more expensive than semi-empirical methods but allow easily studies of medium size molecules [50,51]. The calculated UV spectra

predicts one intense electronic transition at 305.16 nm with an oscillator strength f = 0.1661 a.u and another electronic transition at 426.95 nm with an oscillator strength f = 0.0517 a.u . Calculations of molecular orbital geometry show that the visible absorption maxima of this molecule correspond to the electron transition between frontier orbitals such as translation from HOMO-LUMO [52] . The λ_{max} is a function of substitution. The stronger the donor character of the substitution, the more electrons pushed into the molecule, the larger λ_{max}. These values may be slightly shifted by solvent effects. The role of substituent and role of the solvent influence the UV-Visible spectrum. Both the (HOMO) and (LUMO) are the main orbitals that take part in chemical stability [53].

TABLE 4.Theoretical electronic absorption spectra values of 4A3NP

Excited State	Energy (eV)	Wavelength λ (nm)	Oscillator strengths (f)
Excited State:1	2.7319	453.84	0.0001
Excited State:2	2.9211	426.95	0.0517
Excited State:3	3.0648	404.55	0.0003
Excited State:4	3.5763	346.68	0.0001
Excited State:5	4.0496	305.16	0.1661
Excited State:6	4.7976	258.43	0.0345

4.5 Mulliken charges

The atomic charge in molecules is fundamental to chemistry. For instance, atomic charge has been used to describe the processes of electro negativity equalization and charge transfer in chemical reactions [54,55], and to model the electrostatic potential outside molecular surfaces [56-58]. Mulliken atomic charges calculated at the B3LYP/6-311++ G(d,p) method is collected in Table 5 along with the natural atomic charges obtained in NBO analysis.

TABLE 5. Atomic charges for optimized geometry of 4A3NP using DFT B3LYP/6-31g(d,p)

Atomic Number	4-Amino-3-nitropyridine	
	Mulliken Atomic	Natural atomic
N1	-0.085135	-0.47131
C2	0.00567	0.11023
C3	-0.128977	0.0117
C4	-0.156714	0.21338
C5	0.326244	-0.28471
C6	-0.484519	0.09709
N7	-0.281111	0.39379
N8	-0.322698	-0.76186
H9	0.162766	0.22614
H10	0.185045	0.20125
H11	0.251401	0.23116
O12	-0.025552	-0.36602
O13	-0.027816	-0.41341
H14	0.309034	0.42934
H15	0.272361	0.38322

It is worthy to note that C2 and C5 atoms of 4A3NP exhibit positive charge, while C3,C4 and C6 atoms exhibit negative charges. C6 atom has a maximum negative charge value of about -0.484519. The maximum positive atomic charge is obtained for C5 having a charge value about 0.326244 which is a carbon atom present in the ring . However all the hydrogen atoms exhibit a net positive charge. Of which H14 connected with N8 atom has maximum charge value about 0.309034. This is due to the presence of electro negative nitrogen of the NH group. Illustration of both mullikken atomic charges and Natural atomic charges were plotted at 6-311++G(d,p) level have been shown in Figure 6 and Figure 7. The histogram of calculated mulliken charges and natural atomic charges of 4A3NP were shown in Figure 8.

The presence of large negative charge on N and O atom and net positive charge on H atom may suggest the formation of intramolecular interaction in solid forms [59].

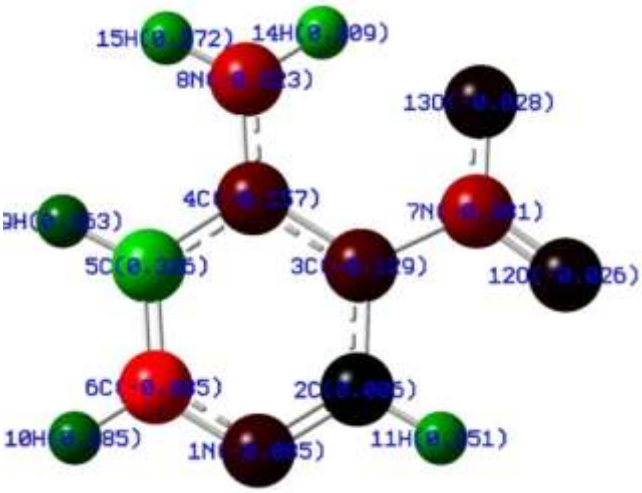

Fig 6.Illustration of mullikken atomic charges

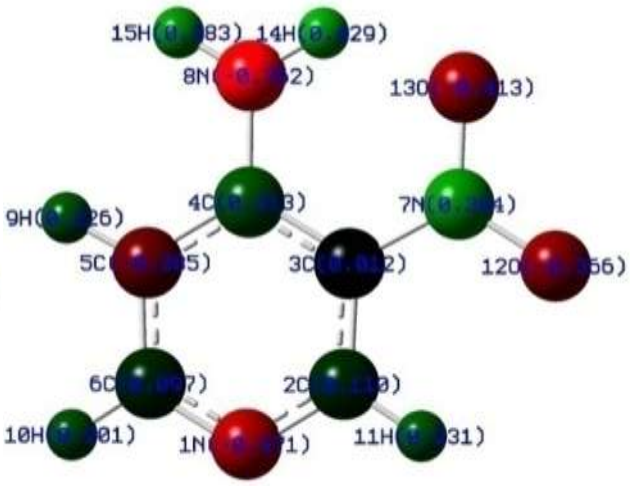

Fig 7. Illustration of Natural atomic charges

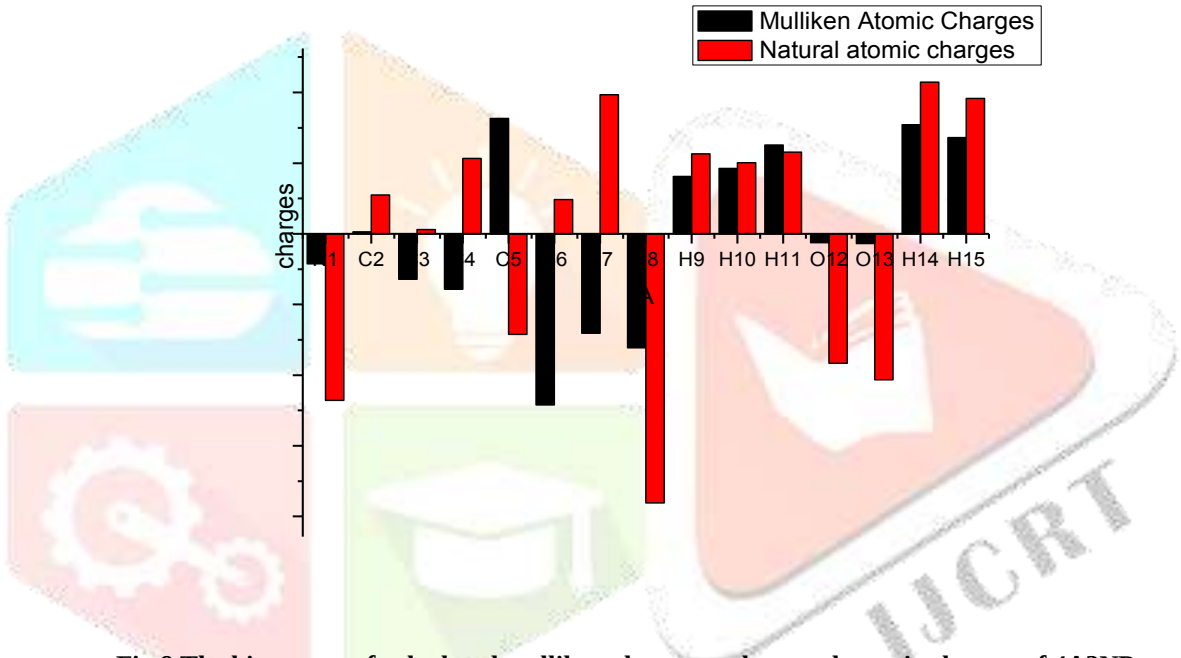

Fig 8.The histogram of calculated mulliken charges and natural atomic charges of 4A3NP

4.6. ^{13}C and ^{1}H NMR spectral analysis

Gauge Invariant Atomic Orbital's (GIAO) NMR DFT calculations can successfully predict the chemical shift (δ, ppm) for small isolated molecules [60-62]. In general only nuclei with odd mass numbers are NMR active (eg ^{1}H, ^{13}C, ^{19}F, ^{31}P) .The accuracy of NMR theoretical predictions depend on the implemented basis set and optimized structural parameters. Therefore, structural parameters obtained with the hybrid B3LYP functional at the 6-311++G(d,p) level of theory were used to predict ^{1}H and ^{13}C chemical shifts utilizing the recommended GIAO approach [63]. Chemical shifts were reported in parts per million relative to TMS(TetraMethylSilane). Relative chemical shifts were estimated by using the corresponding TMS shielding calculated in advance at the same theoretical level as the reference. Aromatic carbons give signals in overlapped areas of the spectrum with chemical shift values from 100 to 150 ppm [64,65] .It can be seen from Table 6, that due to the influence of electronegative nitrogen atom, the chemical shift value of carbon atoms are significantly differing the shift positions in the range 150-165 ppm. Thus, the C6 atom has its chemical shifts at 164.08 ppm. The theoretically computed ^{13}C and ^{1}H NMR spectrum are shown in Figure 9. The chemical shift values of one H atoms in amino group is quite low (≤5ppm) due to the shielding effect. The chemical shift values of all Carbon and Hydrogen atoms were reported in Table 6.

Table6. Theoretical isotropic chemical shift calculated using DFT B3LYP/6-31 G(d,p) (with respect to TMS, All values in ppm) for 4A3NP

Calculated chemical shift (ppm)	
Atom	**B3LYP/6-31G(d,p)**
C2	158.03
C3	149.16
C4	159.34
C5	117.73
C6	164.08
H9	7.09
H10	8.93
H11	9.91
H14	9.78
H15	4.16

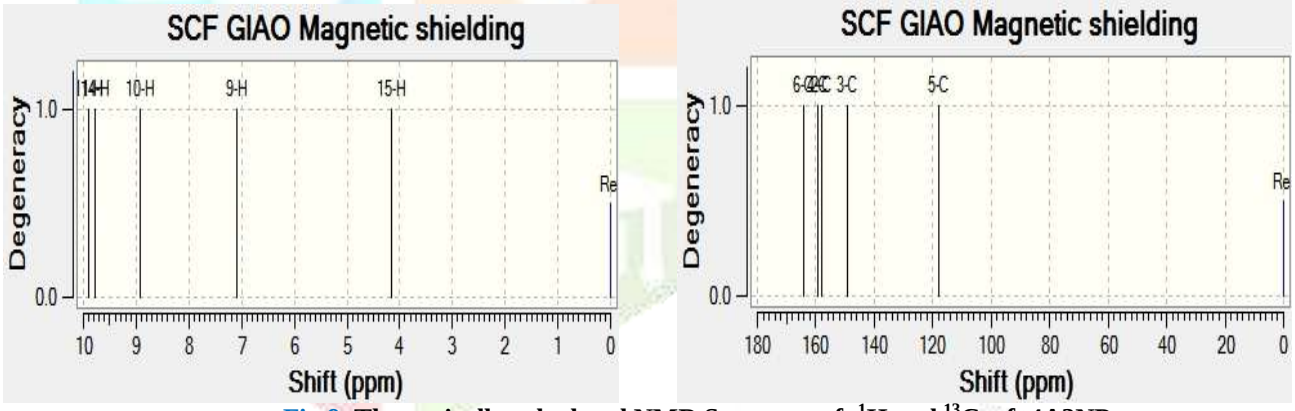

Fig 9. Theoretically calculated NMR Spectrum of ^{1}H and ^{13}C of 4A3NP

4.7 Analysis of molecular electrostatic surface potential

Molecular electrostatic potential (MEP) at a point in space around a molecule gives information about the net electrostatic effect produced at that point by total charge distribution (electron + proton) of the molecule and correlates with dipole moments, electro-negativity, partial charges and chemical reactivity of the molecules. . The molecular electrostatic potential (MEP) at a point r in the space around a molecule (in atomic units) can be expressed as

$$V(r) = \sum_{A} \frac{Z_A}{|\vec{R}_A - \vec{r}|} - \int \frac{\rho(\vec{r}')}{|\vec{r}' - \vec{r}|} \vec{d}r' \qquad (3)$$

Where Z_A is the charge of nucleus A located at R_A, $\rho(\vec{r}')$ is the electronic density function of the molecule, and $\vec{r}'$ is the dummy integration variable.The first and second term represent the contributions to the potential due to nuclei and electron respectively. V(r) is the net resultant electrostatic effect produced at the point r by both the electrons and nuclei of the molecule.

It provides a visual method to understand the relative polarity of the molecule[66,67]. An electron density isosurface mapped with electrostatic potential surface depicts the size, shape, charge density and site of chemical reactivity of the molecules. Electron density from total scf density mapped with esp shown in Figure 10 illustrates the charge distributions of the molecule 4A3NP three dimensionally. Electrostatic potential from total SCF density mapped with ESP of 4A3NP given in Figure 11. The different values of the electrostatic potential at the surface are represented by different colours; red represents regions of most electronegative electrostatic potential, blue represents regions of the most positive electrostatic potential and green represents regions of zero potential. Potential increases in the order red < orange < yellow < green < blue. Blue indicates the strongest

attraction and red indicates the strongest repulsion. Regions of negative potential are usually associated with the lone pair of electronegative atoms [68] . As can be seen from the MESP map of the title molecule, negative region are mainly localized over nitrogen in the ring and oxygen atom in the nitro group. That is negative potential sites are on the electronegative atoms while the positive potential sites around the hydrogen and carbon atoms. The maximum positive region is localized on the hydrogen atom of amino group. Green area covers parts of the molecule where electrostatic potentials are nearly equal to zero (C-C bond). This is a region of zero potential enveloping the π systems of aromatic ring leaving a more electrophilic region in the plane of hydrogen atom. The electrostatic potential contour map of positive and negative potential is shown in Figure 12

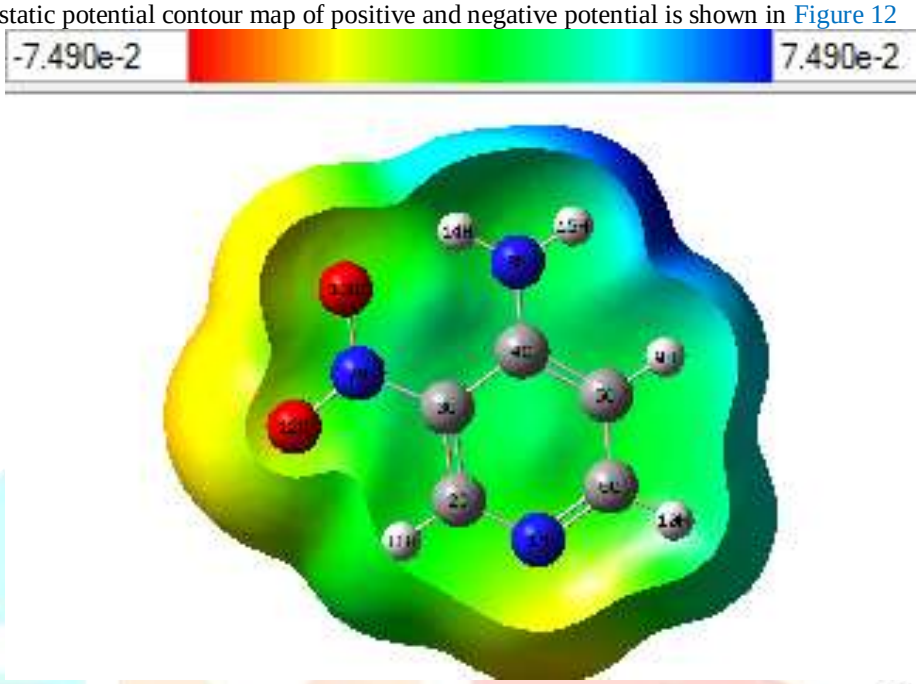

Fig 10. Electron Density From Total SCF Density Mapped With ESP of 4A3NP

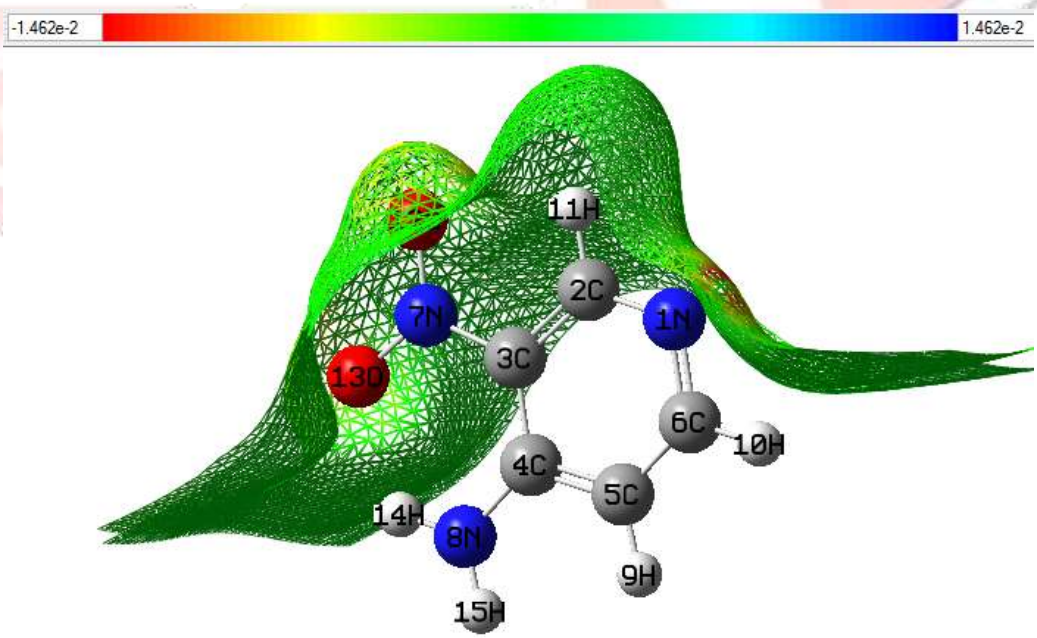

Fig 11. Electrostatic potential from total SCF density mapped with ESP of 4A3NP

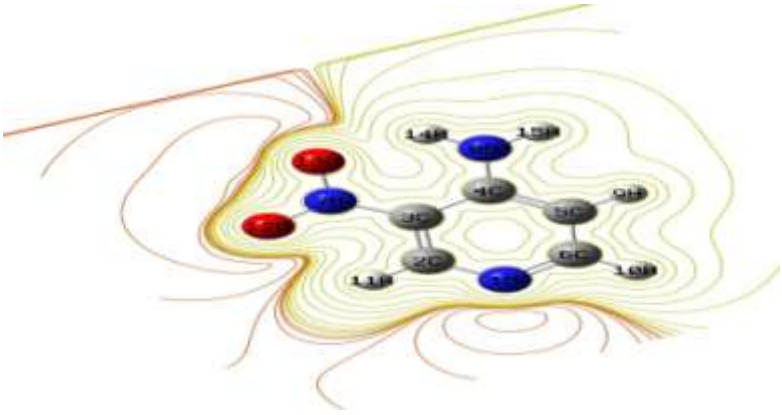

Fig 12. Contour map of molecular electrostatic potential surface

5. Global reactivity descriptors

The chemical hardness is a measure of resistance to charge transfer while the electro negativity is a measure of the tendency to attract electrons by an atom in a chemical bond which is defined as the negative of the chemical potential in DFT. Total dipole moment imitates the ability of interaction of compounds with the surrounding medium.

On the basis of HOMO and LUMO energy values for a molecule, the global chemical reactivity descriptors of molecules such as hardness (η), chemical potential (μ), softness (S), electronegativity (χ) and electrophilicity index (ω) have been defined [69,70].

Physical hardness measures the resistance to change of the nuclear positions in a system. An equilibrium state should have the greatest resistance to change for both properties.While The chemical potential of the molecule is the change in internal energy (at constant S,V) when one mole of the substance is added or removed. Particles tend to flow from a system with a high value of chemical potential (μ_1) to a system with a low value of chemical potential (μ_2). This particle transfer continues until $\mu_1 = \mu_2$.

Using Koopman's theorem for closed-shell molecules, The chemical hardness($\boldsymbol{\eta}$) of the molecule is defined as [71]

$$\eta = \frac{(I-A)}{2} \qquad (5.1)$$

Where I is the ionization potential and A is the electron affinity of the molecule. I and A can be expressed through HOMO and LUMO orbital energies as I = - E_{HOMO} and A = - E_{LUMO}.

The equation of chemical potential (μ) in terms of HOMO and LUMO is

$$\mu = -\frac{(I-A)}{2} \qquad (5.2)$$

The softness (S)of the molecule is given by the equation

$$S = \frac{1}{2\eta} \qquad (5.3)$$

The electronegativity (χ)of he molecule is represented by the equation

$$\chi = \frac{(I+A)}{2} \qquad (5.4)$$

The electrophilicity(**ω**) index of the molecule can be found out by equation

$$\boldsymbol{\omega} = \frac{\boldsymbol{\mu^2}}{\boldsymbol{2\eta}} \qquad (5.5)$$

The ionization potential I of the title molecule 4A3NP calculated by B3LYP/ 6-311++G(d,p) method is 7.3498 eV and electron affinity A of title molecule 4A3NP is calculated as 3.4559 eV.

TABLE 7.Energy values of 4A3NP by B3LYP/6 31g(d,p) method

Energies	Values
E_{HOMO} (eV)	7.3498
E_{LUMO} (eV)	3.4559
E_{HOMO} - E_{LUMO} gap (eV)	3.8939
Chemical hardness (η)	1.9470
Softness (S)	0.2568
Chemical potential (μ)	-5.4029
Electronegativity (χ)	5.4029
Electrophilicity index (ω)	7.4965

The values of the Chemical Hardness was calculated as 1.9470. The Softness, Chemical potential, Electronegativity and Electrophilicity index of our molecule 4A3NP were calculated and tabulated in TABLE 7 . Large HOMO-LUMO gap represent a hard molecule and small HOMO-LUMO gap represents a soft molecule. It is clear that from the Table 9, the title molecule is very hard since it has a large HOMO-LUMO gap. That is it has a large value of chemical hardness or in other words its softness value is very small.

6. Nonlinear optical (NLO) effects

The NLO activity provide the key functions for frequency shifting, optical modulation, optical switching and optical logic for the developing technologies in areas such as communication, signal processing and optical interconnections [72]. This can be essentially traced to the improvement of the performances of the NLO materials. There has been a growing interest in crystal growth process, particularly, in view of the increasing demand for materials for technological applications[73] .The wide range of applicability of single crystals is evident in the fields of semiconductors, polarizers, infrared detectors, solid state lasers, nonlinear optic, piezoelectric, acousto-optic, photosensitive materials and crystalline thin films for microelectronics and computer industries. The growth of single crystals and their characterization towards device fabrication have assumed great importance due to their significance in both academic research and applied research.

The first static hyperpolarizability (β_o) and its related properties (β, α_o and $\Delta\alpha$) have been calculated using B3LYP/6-311G++(d,p) level based on finite field approach. In the presence of an applied electric field, the energy of a system is a function of the electric field and the first hyperpolarizability (β) is a third rank tensor that can be described by a 3×3×3 matrix. The 27 components of the 3D matrix can be reduced to 10 components because of the Kleinman symmetry [74]. The matrix can be given in the lower tetrahedral format. It is obvious that the lower part of the 3×3×3 matrices is a tetrahedral. The components of β are defined as the coefficients in the Taylor series expansion of the energy in the external electric field. When the external electric field is weak and homogeneous, the expansion is given below:

$$E = E_0 - \mu_\alpha F_\alpha - \tfrac{1}{2}\alpha_{\alpha\beta} F_\alpha F_\beta - \tfrac{1}{6}\beta_{\alpha\beta\gamma} F_\alpha F_\beta F_\gamma + \ldots\ldots \quad (6.1)$$

Where E_o is the energy of the unperturbed molecules, F_α is the field at the origin, μ_α ,$\alpha_{\alpha\beta}$ and $\beta_{\alpha\beta\gamma}$ are the components of dipole moment, polarizability and first hyperpolarizability, respectively.

The total static dipole moment μ, the mean polarizability α_o, the anisotropy of the polarizability $\Delta\alpha$ and the mean first hyperpolarizability β_o, using the x, y and z components are defined as:

The Dipole moment is

$$\mu = (\mu^2_x+\mu^2_y+\mu^2_z)^{1/2} \quad (6.2)$$

Static polarizability is

$$\alpha_0 = (\alpha_{xx}+\alpha_{yy}+\alpha_{zz})/3 \quad (6.3)$$

Total polarizability is

$$\Delta\alpha = 2^{-1/2}[(\alpha_{xx}-\alpha_{yy})^2+(\alpha_{yy}-\alpha_{zz})^2+(\alpha_{zz}-\alpha_{xx})^2+6\alpha^2_{xz}]^{1/2} \quad (6.4)$$

First order hyperpolarizability is

$$\beta = (\beta^2_x+\beta^2_y+\beta^2_z)^{1/2} \quad (6.5)$$

Where $\beta_x = (\beta_{xxx}+\beta_{xyy}+\beta_{xzz})$, $\beta_y = (\beta_{yyy}+\beta_{yzz}+\beta_{yxx})$ And $\beta_z = (\beta_{zzz}+\beta_{zxx}+\beta_{zyy})$

$\beta = [(\beta_{xxx}+\beta_{xyy}+\beta_{xzz})^2+(\beta_{yyy}+\beta_{yzz}+\beta_{yxx})^2+(\beta_{zzz}+\beta_{zxx}+\beta_{zyy})^2]^{1/2}$

In Gaussian 09 output the values of the polarizabilities (α) and hyperpolarizability (β) are reported in atomic units (a.u.). Therefore the calculated values have been converted into electrostatic units (esu) (For α: 1a.u. = 0.1482×10^{-24} esu; For β: 1a.u. = 8.639×10^{-33} esu).The mean polarizability (α_o) and total polarizability ($\Delta\alpha$) of our title molecule are -58.711 a.u or -8.701×10^{-24} esu and -172.007 a.u or -25.4915×10^{-24} esu respectively. The total molecular dipole moment and first order hyperpolarizability are 5.355 Debye and 60.6597 au or 524.04×10^{-33} esu, respectively and are depicted in Table 8.Total dipole moment of title molecule is approximately 1.4 times greater than that of urea and first order hyperpolarizability is 3 times greater than that of urea (μ and β of urea are 1.3732 Debye and 0.3728×10^{-30} esu obtained by B3LYP/6-31 G(d,p) method. This result indicates that title molecule 4A3NP has nonlinearity property.

Table 8. The electric dipole moment, polarizability and first order hyperpolarizability 4A3NP

Dipole moment, μ (Debye)		Polarizability α			First order hyperpolarizability β		
Paramet	**Value**	**Parameter**	**a.u.**	**esu(×10^{-24})**	**Param**	**a.u.**	**esu (×10^{-33})**
μ_x	3.0695	α_{xx}	-64.799	-9.60331	β_{xxx}	25.573	220.924
μ_y	4.3882	α_{xy}	4.1221	0.61092	β_{xxy}	20.219	174.668
μ_z	0.0010	α_{yy}	-52.	-7.78455	β_{xyy}	-7.4561	-64.4132
μ_{total}	5.3552	α_{xz}	0.0022	0.00033	β_{yyy}	41.994	362.783
		α_{zz}	-58.806	-8.71512	β_{xxz}	0.0062	0.05356
		α_{yz}	0.0019	0.00028	β_{xyz}	-0.0071	-0.06134
					β_{yyz}	-0.0046	-0.03974
Total Polarizability		$\Delta\alpha$	-172.01	-25.492	β_{xzz}	-10.422	-90.0339
Mean Polarizability		α_o	-58.711	-8.7011	β_{yzz}	-2.0425	-17.6452
					β_{zzz}	-0.0001	-0.00086
					β_{tot}	67.859	586.235
first order hyperpolarizability					β	60.659	524.04

7. Thermodynamic analysis

Our title molecule 4A3NP has a great deal of interest in thermodynamic property analysis. The zero point vibrational energy in Kcal/Mol and rotational constants in GHz obtained for optimized geometry with B3LYP/6-31++ g(d,p) basis set are presented in Table 9. The molecule was considered to be at room temperature (298.15K) and at a pressure of 1atm while performing DFT Calculations

Table 9-The calculated Thermodynamical parameters of 4A3NP

Parameters	B3LYP/6-311++G(d,p)	
Zero-point vibrational energy (Kcal/Mol)	67.29043	
Rotational constants (GHz):	A	2.34144
	B	1.28897
	C	0.83132

Based on the vibrational analysis of title molecule at B3LYP/6-31 ++ G(d,p) basis set, the thermodynamic parameters such as Energy E ,heat capacity at constant volume(C_V),Entropy(S) and enthalpy change (ΔH) were calculated for different temperatures and listed in the Table 10.

Table 10-The Temperature dependence of Thermodynamic parameters of 4A3NP

Temperature [T] (K)	Energy [E] (kCal/mol)	Heat capacity [Cv] (Cal/mol-Kelvin)	Entropy [S] (Cal/mol-Kelvin)	Enthalpy change (kJ/ mol)
100	92.056	14.372	67.422	0.147018
200	102.422	21.131	78.998	0.163853
300	107.278	31.036	90.854	0.171908
400	110.898	41.287	101.768	0.177993
500	115.499	50.496	112.441	0.185642
600	120.946	58.213	122.714	0.194641
700	127.097	64.597	132.489	0.204759
800	133.83	69.916	141.737	0.215806
900	141.052	74.396	150.472	0.227631
1000	148.687	78.203	158.722	0.240115

It can be seen that, when the temperature increases from 100 to 1000 K the thermodynamic functions like Specific heat capacity at constant volume (C_V), Entropy(S) and enthalpy (ΔH) are also increases since molecular vibrational intensities increase with temperature [15] [75]. The entropy and enthalpy changes revealed that the title compound possesses more flexibility of changing its own thermodynamic system with respect to the temperature. Fitting factor of the thermodynamic functions such asEnergy , specific heat heat capacity at constant volume, entropy and enthalpy changes at room temperature are 107.278 kCal/mol 31.036 Cal/mol-Kelvin, 90.854 Cal/mol-Kelvin and 0.171908 kJ/mol respectively. The correlation graphs of temperature dependence of thermodynamic functions for 4A3NPmolecule are shown in Figures 13.

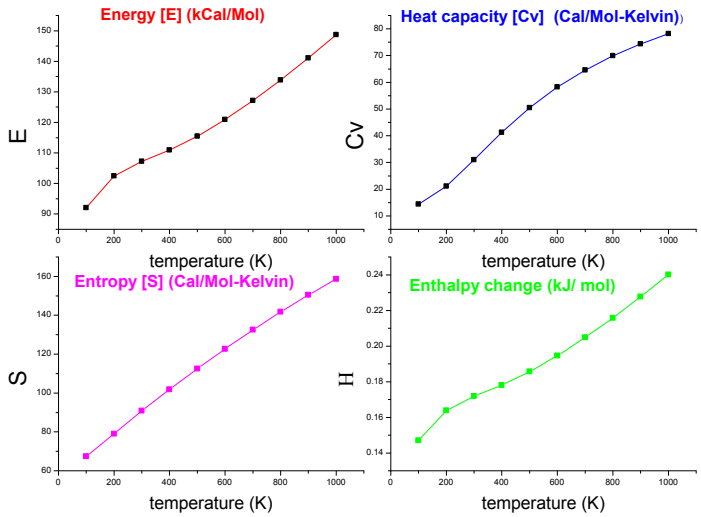

Fig 13.Temperature dependence of Energy E , Heat Capacity At Constant Volume Cv , Entropy S and Enthalpy Change H of 4A3NP

8.1 Molecular docking studies of 4A3NP with the target proteins

Molecular docking is used to predict the structure of intermolecular complex formed between two molecules. The small molecule called ligand (here our title molecule) usually interact with proteins active sites. Auto Dock suite 4.2.6 is a recently been used as an expedient tool to get insights into the molecular mechanism of protein-ligand interactions. The two proteins 4YPO[76] and 5CNJ[77] having anti tuberculosis properties were obtained from the RCSB Protein Data Bank (PDB) since our title molecule shows anti tuberculosis properties which was identified with the help of PASS (Prediction of Activity Spectra) [78], an online tool to predict the activity of a compound. PASS analysis of the title compound predicts anti tuberculosis activity as the most probable activity with Pa value of 0.6 .

Water molecules of crystallization were removed from the complex, and hydrogen atoms were added to the structure and protein was optimized. Partial atomic charges were also assigned according to the force field. Induced fit docking between 4A3NP and each of the target protein (4YPO and 5NCJ) were carried out. The ligand was docked into the functional sites of the respective proteins individually and the docking energy was examined to achieve a minimum value. Auto Dock results indicate the binding position of a rough estimation of their interaction. The hydrogen bond interactions of ligand with amino acids at the active site of two target proteins were given in Table 11. Hydrogen bond interactions of 4A3NP with amino acids at the active site of the two anti tuberculosis target proteins were shown in Figure 14 and Figure 15, respectively.

Binding energy is a measure of the affinity of ligand-protein complex, or it is the difference between the energy of complex and the sum of energies of each molecule separately. Intermolecular energy is the energy between non-bounded atoms that is the energy between atoms in different molecules. Inhibition constant (Ki) is an indication of how potent an inhibitor or enzyme is .The smaller the Ki, the greater the binding affinity and the smaller amount of medication needed in order to inhibit the activity of that enzyme. If a Ki is much larger than the maximal drug concentrations that a patient is typically exposed to from typical dosing, then that drug is not likely to inhibit the activity of that enzyme.

In the case of 4YPO the Estimated Inhibition Constant, Ki is 582.96 uM (micromolar) and a minimum estimated free binding energy of -4.41 kcal/mol and Final Intermolecular Energy of -5.01 kcal/mol were seen in the interaction. Meanwhile In the case of 5NCJ the Estimated Inhibition Constant, (Ki) is 51.26μM (micromolar) and a minimum estimated free binding energy of -5.85 kcal/mol and Final Intermolecular Energy of -6.45 kcal/mol were seen in the interaction. Molecular docking results draw us to the conclusion that the compound might exhibit tuberculosis inhibitory activity.

Table 11. Docked interaction analysis of 4A3NP with target proteins 4YPO and 5NCJ

Ligand	Receptors (PDB ID)	Number of H-bonds	Active site residues	Number of interacting bonds	Bonds length in Å
4A3NP	4YPO	5	SER 50	1	1.7
			SER 48	2	2.8 ,1.9
			LYS 45	2	2.5,2.0
	5NCJ	7	TYR 59	1	2
			GLN 93	2	2.7,1.8
			TRP 116	1	2.3
			ARG 242	2	2.2,2.1
			VAL 170	1	2

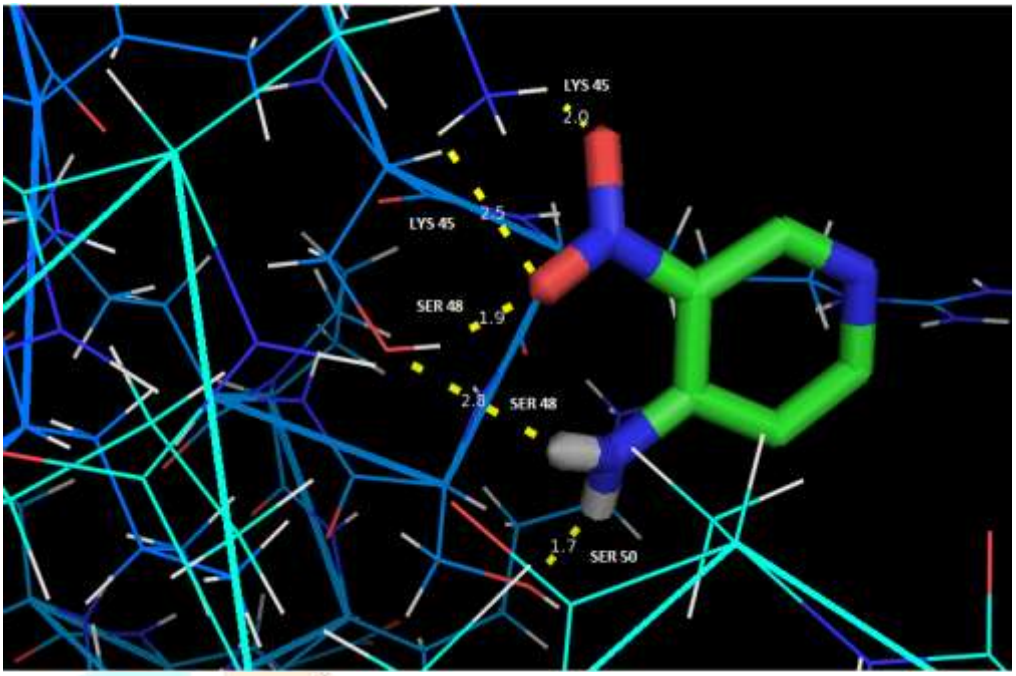

Fig. 13- Hydrogen bond interactions of 4A3NP with amino acids at the active site of the target protein 4YPO

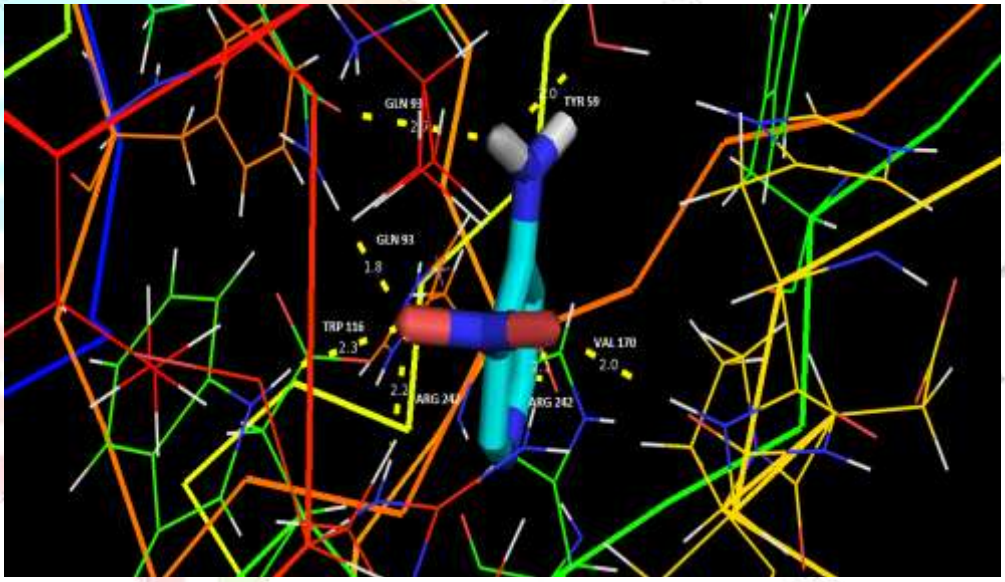

Fig. 14- Hydrogen bond interactions of 4A3NP with amino acids at the active site of the target protein 5NCJ

8.2 Drug Likeness and bioactivity of ligand molecule 4A3NP

Druglikeness may be defined as a complex balance of various molecular properties and structure features which determine whether particular molecule is similar to the known drugs. These properties, mainly hydrophobicity, electronic distribution, hydrogen bonding characteristics, molecule size and flexibility and of course presence of various pharmacophoric features influence the behavior of molecule in a living organism, including bioavailability, transport properties, affinity to proteins, reactivity, toxicity, metabolic stability and many others. Lipinski rule states that most drug like molecules have logp ≤ 5, Molecular weight≤ 500, No of Hydrogen bond acceptors ≤ 10, No of Hydrogen bond donors ≤ 5. Molecules violating one of these rules may have problem with bioactivity[79,80].this rule is called rule of five since the boarder values are 5,500, 2*5=10 and 5. The molecular properties, Drug likeness and the prediction of bioactivity of the ligand was calculated using Molinspiration tool [81] and listed in Tables 12 and Table 13 respectively. It was found that the ligand molecule 4A3NP satisfies the 'rule of 5' and could be a potent inhibitor.

Table 12 Molecular properties of 4A3NP

Property	Details	values
Log P	Octanol-water patition coefficient	0.24
TPSA	Polar Surface Area	84.74
natos	Number of non hydrogen atom	10
MW	Molecular Weight	139.11
nON	No of Hydrogen bond acceptors(O and N atoms)	5
nOHNH	No of Hydrogen bond donors(OH and NH groups)	2

nviolations	No of rule of five violations	0
nrotb	No of rotatble bonds	1
Volume	Molecular volume	114.51

Table 13 Bio activity score and drug likeness of 4A3NP by Molinspiration tool

GPCR ligand	-1.21
Ion channel modulator	-0.21
Kinase inhibitor	-0.80
Nuclear receptor ligand	-1.76
Protease inhibitor	-1.29
Enzyme inhibitor	-0.37

9. Conclusion

Based on Scaled Quantum Mechanical force field obtained by DFT calculations at B3LYP/6-311+ g(d,p) level a complete structural information ,FT-IR and FT-Raman vibrational analysis ,electronic properties and vibrational properties of 4A3NP have been carried out. The molecular geometry, vibrational frequencies, infrared intensities Raman activities and Raman intensities of 4A3NP are calculated. The theoretically calculated vibrational modes are compared with experimental values. Even in the low frequency region the experimental values are in good agreement with theoretical values. The difference between the observed and scaled wave number values of most of the fundamentals is very small. The theoretical UV-Visible spectrum was recorded. The ^{1}H and ^{13}C NMR magnetic isotropic chemical shifts were calculated by B3LYP/6-311++ g(d,p) basis set . Total dipole moment, Rotational constants, total energy ,entropy, heat capacity at constant volume, zero point vibrational energy and SCF energy of title compound are calculated. The difference in HOMO and LUMO energy supports the interaction of charge transfer within the molecule. The MEP map shows that the negative potential sites are around Nitrogen atoms as well as the positive potential sites are around the hydrogen atoms. The greater dipole moment and hyperpolarizability of the title molecule shows the large NLO optical property of the title molecule. The thermodynamic properties (heat capacity at constant volume, entropy and enthalpy changes) in the temperature ranges from 100 to 1000 K ,Rotational constants, a zero point vibrational energy and SCF energy of title compound are calculated are also calculated. Molecular docking results draw us to the conclusion that the compound might exhibit tuberculosis inhibitory activity. It was found that the ligand molecule 4A3NP satisfies the 'rule of 5' and could be a potent inhibitor of tuberculosis. However biological test need to be done to validate the computational predictions.

Acknowledgement

The authors are thankful to Sophisticated Analytical Instrumentation Facility (SAIF), IIT, Chennai, for the spectral measurements.

REFERENCE

[1] Th. Zeegers-Huyskens, P. Huyskens, H. Ratajczak, W.J. Orville-Thomas (Eds.), Molecular Interactions, vol. 2, Wiley, Chichester, UK, 1981, p. 1.
[2] E.N. Gur'yanova, I.P. Gol'dshtein, T.I. Perepelkova, Russ. Chem. Rev. 45 (1976) 792 806.
[3] S. Tomaru, S. Matsumoto, T. Kurihara, H. Suzuki, N. Oobara, T. Kaino, Appl. Phys. Lett. 58 (1991) 2583–2585.
[4] C. Kaneko, S. Yamada, I. Yokoe, N. Hata, Y. Ubata, Tetrahedron Lett. 7 (1966) 4729–4733.
[5] C. Kaneko, I. Yokoe, S. Yamada, Tetrahedron Lett. 8 (1967) 775–778.
[6] N. Hata, E. Okutsu, I. Tanaka, Bull. Chem. Soc. Jpn. 41 (1968) 1769–1775.
[7] N. Hata, I. Ono, T. Tuchiya, Bull. Chem. Soc. Jpn. 45 (1972) 2386–2391.
[8] I. Ono, N. Hata, Bull. Chem. Soc. Jpn. 45 (1972) 2951–2953.
[9] D. Dopp, in: Davidson (Ed.), Topics in Current Chemistry, vol.55,Springer,Berlin,1975,p. 49.
[10]Motte Tollet F Eustatiu G & Roy D, J Chem Phys,105 (1996) 7448.
[11]Hajduk, P.H.,Bures,M.,Praestgaard,J.,and Fesik, S.W.,J. Med. Chem., 2000, vol. 43, p. 3443.
[12]Labrie, F., Singh, Sh.M., and Vab Luu-The, USA Patentno. 6933321, 2005..
[13]S.P. Jose, S. Mohan, Spectrochim. Acta 64A (2006) 240–245.
[14]Kirk-Othmer, in: M. Howe-Grant (Ed.), Kirk-Othmer Encyclopedia of Chemical Technology, Vol. 1, 4th ed., John Wiley and Sons, New York, 1997, p. 20.
[15]P. Pierrat, P.C. Gros, Y. Fort, J. Comb. Chem. 7 (2005) 879–886.
[16]X. Chao, X. Zhang, K. Wang, J. Ji and Q. Chen Acta Cryst. (2012). E68, o114.
[17]P. Hohenberg, W. Kohn, Phys. Rev. 136 (1964) B864–B871.
[18]A.D. Becke, J. Chem. Phys. 98 (1993) 5648–5652.
[19]C. Lee, W. Yang, R.G. Parr, Phys. Rev. B 37 (1988) 785–789.
[20]M.J. Frisch, G.W. Trucks, H.B. Schlegel, G.E. Scuseria, M.A. Robb, J.R. Cheeseman, J.A. Montgomery Jr., T. Vreven, K.N. Kudin, J.C. Burant, J.M. Millam, S.S. Iyengar, J. Tomasi, V. Barone, B. Mennucci, M. Cossi, G. Scalmani, N. Rega, G.A. Petersson, H. Nakatsuji, M. Hada, M. Ehara, K. Toyota, R. Fukuda, J. Hasegawa, M. Ishida, T. Nakajima, Y. Honda, O. Kitao, H. Nakai, M. Klene, X. Li, J.E. Knox, H.P. Hratchian, J.B. Cross, C. Adamo, J. Jaramillo, R. Gomperts, R.E. Stratmann, O. Yazyev, A.J. Austin, R. Cammi, C. Pomelli, J.W. Ochterski, P.Y. Ayala, K. Morokuma, A. Voth, P. Salvador, J.J. Dannenberg, V.G. Zakrzewski, S. Dapprich, A.D. Daniels, M.C. Strain, O. Farkas, D.K. Malick, A.D. Rabuck, K. Raghavachari, J.B. Foresman, J.V. Ortiz, Q. Cui, A.G. Baboul, S. Clifford, J. Cioslowski, B.B. Stefanov, G. Liu, A. Liashenko, P. Piskorz, I. Komaromi, R.L. Martin, D.J. Fox, T. Keith, M.A. Al-Laham, C.Y. Peng, A. Nanayakkara, M.

Challacombe, P.M.W. Gill, B. Johnson, W. Chen, M.W. Wong, C. Gonzalez, J.A. Pople, Gaussian Inc., Wallingford, CT, 2009.
[21]H.B. Schlegel, J. Comput. Chem. 3 (1982) 214–218
[22]V. Mukherjee, N.P. Singh, R.A. Yadav, J. Mol. Struct. 988 (2011) 24–34.
[23]G. Rauhut, P. Pulay, J. Phys. Chem. 99 (1995) 3093–3100.
[24]P. Pulay, G. Fogarasi, G. Pongor, J.E. Boggs, A. Vargha, J. Am. Chem. Soc. 105 (1983) 7037–7047.
[25]G. Fogarasi,P. Pulay, in:J.R.Durig (Ed.),Vibrational Spectra and Structure, vol.14, Elsevier, Amsterdam, 1985, pp. 125–219.
[26]T. Sundius, J. Mol. Struct. 218 (1990) 321–326.
[27] T. Sundius, Vib. Spectrosc. 29 (2002) 89–95.
[28] G. Keresztury, S. Holly, G. Besenyei, J. Varga, A. Wang, J.R. Durig, Spectrochim. Acta 49 (1993) 2007–2026.
[29]G. Keresztury, in: J.M. Chalmers, P.R. Griffth (Eds.), Raman Spectroscopy: Theory in Handbook of Vibrational Spectroscopy, vol. 1, John Wiley & Sons Ltd., New York, 2002, pp. 71–87.
[30] N.B. Colthup, L.H. Daly, S.E. Wiberley, Introduction to Infrared and Raman Spectroscopy, Academic Press, New York, 1964. pp. 226;
[31]N. Sundaraganesan, Dominic Joshua, C. Meganathan & S. Sebastian, Indian J.Chem, Sec A (47A) (2008) 821-829.
[32]M. Arivazhagan, V. Krishna Kumar, R. John Xavier, G. Ilango and V. Balachandran, Spectrochim. Acta, A72 (2009)941-946.
[33] G. Socrates, Infrared and Raman Characteristic Group Frequencies, 3rd ed., John Wiley and Sons Ltd., Chichester, (2001)PP .50-67.
[34]T. Vijayakumar, I. Hubertjoe, C.P.R. Nair, V.S. Jayakumar, Chem. Phys. 343 (2008) 83–89.
[35]B. Wojtkowaik, M. Chabanel, Spectrochimie Moleculaire Technique et Docu-mentation, Paris, 1977, p. 265.
[36]H. Baraistka, A. Labudzinska, J. Terpinski, Laser Raman Spectroscopy: Analyt-ical Applications, PWN – Polish Scientific Publishers/Ellis Harwood Limited Publishers, 1987.
[37]N. Sundaraganesan , C. Meganathan , Mustafa Kurt .Journal of Molecular Structure 891 (2008) 284–291
[38]G. Socrates, Infrared and Raman Characteristic group frequencies, Tables and Charts, third ed., Wiley, Chichester, 2001
[39]F.R. Dollish, W.G. Fateley, F.F. Bentley, Characteristic Raman Frequencies of Organic Compounds, John Wiley & Sons, New York, 1997.
[40]G. Fogarasi, X. Zhou, P.W. Taylor,P. Pulay,J. Am. Chem. Soc. 114(1992) 8191– 8201
[41]Mehmet Karabacak, Mehmet Cinar, Mustafa Kurt, Spectrochim. Acta Part A Mol. Biomol. Spectrosc. 74 (2009) 1197–1203.
[42]K. Fukui, Science 218 (1982) 747–754.
[43]K. Fukui, T. Yonezawa, H. Shingu, J. Phys. Chem. 20 (1952) 722–725.
[44]M. Kurt, P. ChinnaBabu, N. Sundaraganesan, M. Cinar, M. Karabacak, Spectrochim. Acta Part A 79 (2011) 1162–1170.
[45] L. Padmaja, C. Ravikumar, D. Sajan, I.H. Joe, V.S. Jayakumar, G.R. Pettit, O.F. Nielsen, J. Raman Spectrosc. 40 (2009) 419–428.
[46]C. Ravikumar, I.H. Joe, V.S. Jayakumar, Chem. Phys. Lett. 460 (2008) 552–558
[47]D. Jacquemin, J. Preat, E.A. Perpete, Chem. Phys. Lett. 40 (2005) 254-259.
[48]D. Jacquemin, J. Preat, M. Charlot, V. Wathelet, J.M. Andre, E.A. Perpete, J. Chem. Phys. 121 (2004) 1736-1744.
[49]M. Cossi, V. Barone, J. Chem. Phys. 115 (2001) 4708-4717.
[50]D. Guillaumont, S. Nakamura, Dyes Pigments 46 (2000) 85–92.
[51]J. Fabian, Dyes Pigments 84 (2010) 36–53
[52]M. Kurt, P. ChinnaBabu, N. Sundaraganesan, M. Cinar, M. Karabacak, Spectrochim. Acta Part A 79 (2011) 1162–1170.
[53]S. Gunasekaran, R.A. Balaji, S. Kumeresan, G. Anand, S. Srinivasan, Can. J. Anal. Sci. Spectrosc. 53 (2008) 149-161.
[54]K. Jug, Z.B. Maksic, in: Z.B. Maksic (Ed.), Theoretical Model of Chemical Bonding, Part 3, Springer, Berlin, 1991, p. 233.
[55]S. Fliszar, Charge Distributions and Chemical Effects, Springer, New York, 1983.
[56]P.E. Smith, J. Am. Chem. Soc. 113 (1991) 6029–6037.
[57]J. Gao, J. Chem. Phys. 98 (1993) 1975–1981.
[58]P. Cieplak, J. Comp. Chem. 12 (1991) 1232–1236.
[59]L. Xiao-Hong, et al., Comput. Theor. Chem. 969 (2011) 27–34.
[60]V.G. Malkin, O.L. Malkina, M.E. Casida, D.R. Salahub, J. Am. Chem. Soc. 116 (1994) 5898–5908.
[61]D.B. Chesnut, C.G. Phung, J. Chem. Phys. 91 (1989) 6238–6245.
[62]T. Kupka, M. Kolaski, G. Pasterna, K. Ruud, J. Mol. Struct. THEOCHEM 467 (1999) 63–78.
[63]H.O. Kalinowski, S. Berger, S. Braun, Carbon-13 NMR Spectroscopy, John Wiley&Sons, Chichester, 1988.
[64]K. Pihlaja, E. Kleinpeter (Eds.), Carbon-13 Chemical Shifts in Structural and Sterochemical Analysis, VCH Publishers, Deerfield Beach, 1994.
[65]D. Arul Dhas, I. Hubert Joe, S.D.D. Roy, T.H. Freeda, Spectrochim. Acta 77 (2010) 36–44.
[66]S. Chidangil, M.K. Shukla, P.C. Mishra, J. Mol. Model. 4 (1998) 250–258.
[67]F.J. Luque, J.M. Lopez, M. Orozco, Theor. Chem. Acc. 103 (2000) 343–345.
[68]Y. Sheena Mary a, C. Yohannan Panicker b, M. Sapnakumari c, B. Narayana c, B.K. Sarojini d, Abdulaziz A. Al-Saadi e, Christian Van Alsenoy f, Javeed Ahmad War g Spectrochimica Acta Part A: Molecular and Biomolecular Spectroscopy 138 (2015) 73–84
[69]Z. Parr, L. Szentpaly, S. Liu, Am. Chem. Soc. 121 (1999) 1922–1924.
[70]P. C hattraj, B. Maiti, U. Sarkar, J. Phys. Chem. A107 (2003) 4973–4975.
[71]S.Seshadri, Rasheed.M.P ,R.Sangeetha ,IOSR-J. Appl.Chem 8(2015) 87-100

[72]C. Andraud, T. Brotin, C. Garcia, F. Pelle, P. Goldner, B. Bigot, A. Collet, J. Am. Chem. Soc. 116 (1994) 2094–2101
[73]D.A. Kleinman, Phys. Rev. 126 (1977) 1962–1979.
[74]D.A. Kleinman, Phys. Rev. 126 (1977) 1962–1979.
[75]J.B. Ott, J. Boerio-Goates, Chemical Thermodynamics: Advanced Applications, Calculations from Statistical Thermodynamics, Academic Press 2000.
[76]PDB ID: 4YPO ;Lv, Y., Kandale, A., Wun, S.J., McGeary, R.P., Williams, S.J., Kobe, B., Sieber, V., Schembri, M.A., Schenk, G., Guddat, L.W.(2016) Febs J 283 1184-1196
[77]PDB ID :5NCJ ; Lukat, P., Katsuyama, Y., Wenzel, S., Binz, T., Koenig, C., Blankenfeldt, W., Broenstrup, M., Mueller, R.(2017) Chem Sci DOI: 10.2210/pdb5ncj/pdb
[78]A. Lagunin, A. Stepanchikova, D. Filimonov, V. Poroikov, Bioinformatics 16 (2000)747-748
[79]Lipinski, C.A., Lombardo, F., Dominy, B.W. and Feeney, P.J. (1997) Experimental and Computational Approaches to Estimate Solubility and Permeability in Drug Discovery and Development Settings. Advanced Drug Delivery Reviews, 23, 3-25.
[80] Lipinski, C.A Drug-like properties and the causes of poor solubility and poor permeability. J Pharmacol Toxicol Methods 2000 Jul-Aug;44(1):235-49
[81] http://www.molinspiration.com